An Accurate Numerical Scheme for Maxwell Equation with CIP-Method of Characteristics

Youichi Ogata[1], Takashi Yabe[1,*] and Kouichi Odagaki[1]

[1] *Department of Mechanical Sciences and Engineering, Tokyo Institute of Technology, 2-12-1 Meguro-ku, Ookayama 152-8552, Japan.*

Abstract. A new multi-dimensional scheme for the Maxwell equations is established by the CIP method in combination with the method of characteristics (CIP-MOC). In addition, the CIP-MOC can be extended to arbitrary grid system by the Soroban grid without losing the third-order accuracy. With the accuracy fixed, the grid points required for the CIP are 40 times less than the conventional schemes like the FDTD in three dimensions. Numerical solutions obtained by the CIP-MOC are compared with analytical solution and the FDTD in plane-wave scattering by a perfectly-conducting circular cylinder, and the CIP-MOC agrees very well with analytical solutions. The Soroban grid is also applied to the Vlasov equation that describes the kinematics of plasmas that is frequently combined with the Maxwell equation. The adaptively moving points in velocity space are similar to the particle codes but can provide accurate solutions.

Key words: Maxwell equation; Vlasov equation; CIP method; method of characteristics; Soroban grid.

1   Introduction

Although the research of electromagnetic waves has a long history, there is still growing interest in its numerical solution under complex shape boundary as well as material properties of structures and so on. At the frontier of such simulation, we need a reliable numerical schemes that can provide the correct prediction even for a new regime not explored before. Owing to unknown reliability of the numerical solutions, the details of many unknown data are estimated on the basis of some experimental measurements.

---

*Correspondence to: Takashi Yabe, Department of Mechanical Sciences and Engineering, Tokyo Institute of Technology, 2-12-1 Meguro-ku, Ookayama 152-8552, Japan. Email: `yabe@mech.titech.ac.jp`

However, it is obvious that such empirical law obtained by measurements is not flexible and it requires a lot of efforts and time. Therefore, in order to effectively cope with all kinds of complex and usual phenomena, numerical analysis has been attracting attention in order to overcome these problems. Since performance of computers has been increasing these days, this option will be very promising for electromagnetic field analysis once a reliable scheme is established.

A number of numerical schemes have been developed from a continuum version of the Maxwell equations to a discretized version by using various differencing schemes in time and space. Some of the well-known schemes are the Finite-Difference Time-Domain (FDTD) method [1], the Finite Element Method (FEM) [2], and so forth. The ray-tracing method can be applied to refraction and reflection on the material surface, however, when there are some complicated structures in a domain, the number of lights that have to be traced becomes huge.

The FDTD method has been commonly used because it is very easy to make the program and treat current sources, dielectrics and conductors consistently. Since this scheme has already been established for a long time, it has been employed for all kinds of commercial software.

However, the FDTD method is the second order in time and space and its phase error is quite large in short wavelength component. Since electromagnetic waves are composed of arbitral wavelengths or frequencies and the numerical resolution of wave motions is determined from the minimum wave number within the frequency spectrum, the required number of grid should be enormous in order to provide adequate numerical resolution beyond the Rayleigh into the resonance.

Therefore, the application of the CIP method [3–6] to the analysis of computational electromagnetics seems to be promising because of its non-dispersive characteristics. Since the CIP method can accurately solve the hyperbolic equations and the Maxwell equations are also a system of hyperbolic partial differential equations (PDEs) , the CIP method can be similarly applied to the propagation of characteristics that appears in electromagnetic waves.

The objective of this study is to explore the benefits of using the theory of characteristics in developing accurate and efficient numerical algorithms for computational electromagnetics. The present work adopts the CIP method in combination with the numerical method of characteristics (MOC). Hereafter, it is called the CIP-MOC method. We have already applied the CIP-MOC method to the multi-dimensional shallow water equations [7] with directional splitting, and the same procedure can be applied to the Maxwell equations as well.

Although the CIP is the third-order in time and space in uniform grid, the accuracy of any schemes including the CIP becomes the first-order in time and space for abruptly changing the size of meshes once the metric tensors for coordinate transformation are estimated by finite difference methods. In order to resolve this problem, a new body-fitted grid system, the Soroban-grid was proposed in the previous paper [8]. One of the advantages of the Soroban grid is that it can keep the third-order accuracy in time and

space even in deformed mesh because it does not have to use coordinate transformation that is the main cause of deteriorating accuracy. This new scheme is also like a mesh-free scheme, or it seems to be similar to the point interpolation method among the mesh-free schemes [9]. In contrast to these mesh-free schemes, however, the Soroban grid is able to determine multi-dimensional CIP interpolation without shape functions or solving moment matrix, and therefore we can easily construct a very accurate Maxwell solver with the CIP-MOC method. The basic concept of the CIP-MOC is introduced in Section 2, and the CIP-MOC in multi-dimensions will be explained in Section 3. The advantages of the CIP-MOC and the Soroban grid will be discussed in Section 4.

Sometimes the Maxwell equations are coupled with the Vlasov equation that determines the kinetic motion of plasmas. Section 5 is devoted to the solution of such equation in the Soroban grid.

2 CIP method for Maxwell equations

2.1 Basic CIP-MOC algorithm in one dimension

When we analyze the Maxwell equations, there are some dielectrics or conductors in simulation domain in general. In this section, the basic CIP-MOC algorithm in one dimension is introduced. The Maxwell equations for linear, homogeneous and dissipative media with conductor in the one-dimensional TE (Transverse Electric) mode can be described as

$$\frac{\partial E_y}{\partial t} + \frac{1}{\epsilon}\frac{\partial H_z}{\partial x} \;=\; -\frac{\sigma}{\epsilon}E_y, \tag{2.1}$$

$$\frac{\partial H_z}{\partial t} + \frac{1}{\mu}\frac{\partial E_y}{\partial x} \;=\; 0, \tag{2.2}$$
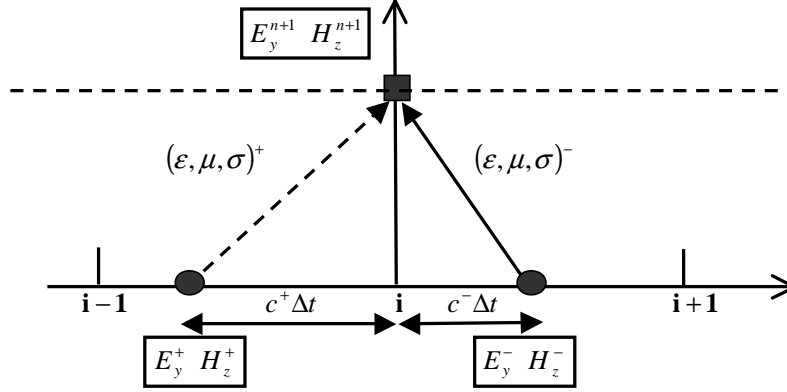
where ϵ, μ and σ are the permittivity, permeability and the electrical conductivity, respectively. We can use the same argument for the TM (Transverse Magnetic) mode as well.

The basic equations Eqs. (2.1) and (2.2) can put into the following form.

$$\frac{D^{\pm}E_y}{Dt} \pm \sqrt{\frac{\mu}{\epsilon}}\frac{D^{\pm}H_z}{Dt} = -\frac{\epsilon}{\sigma}E_y, \quad C^{\pm}: \frac{D^{\pm}}{Dt} = \frac{\partial}{\partial t} + c^{\pm}\frac{\partial}{\partial x}, \tag{2.3}$$

where $c^{\pm} = \pm 1/\sqrt{\epsilon^{\pm}\mu^{\pm}}$ is the speed of light in each medium. This form was originally proposed by Beggs [10].

Unlike the case of free space in which there is no dielectrics and metals, there will be a discontinuity between two different materials as in Fig. 1 and the differences the speed of light, conductivity and so on between two materials , have to be taken into account in numerical algorithms. Therefore, we should use the intrinsic impedance, the speed of light and the conductivity of each material for left (+) and right (-) characteristics, respectively. The characteristics speed on the right half space in Fig. 1 is different from the one on the left half space $dx^{\pm} = \pm c^{\pm}dt$, where $c^{\pm} = 1/\sqrt{\epsilon^{\pm}\mu^{\pm}}$ are the speed of light on both sides.

Figure 1: The characteristic curve that includes dielectrics and conductors in (x-t) plane.

The other subject is how to deal with the right hand side of Eq. (2.3). The exact integration of Eq. (2.3) along the characteristics curves can be expressed as

$$E_y^{n+1} - E_y^{\pm} \pm \sqrt{\frac{\mu^{\pm}}{\epsilon^{\pm}}} \left(H_z^{n+1} - H_z^{\pm} \right) = -\frac{\sigma^{\pm}}{\epsilon^{\pm}} \int_0^{\Delta t} E_y \left(x - c^{\pm}s, t + s \right) ds, \qquad (2.4)$$

where (+) and (-) mean the upstream departure points of the characerics in Fig. 1. The simplest approximation for the integral is the time-averaged value between $\pm$ and $n+1$ step as follows.

$$E_y^{n+1} - E_y^n \pm \sqrt{\frac{\mu^{\pm}}{\epsilon^{\pm}}} \left(H_z^{n+1} - H_z^n \right) = -\frac{\sigma^{\pm}}{\epsilon^{\pm}} [(1 - \lambda) E_y^{n+1} + \lambda E_y^{\pm}], \qquad (2.5)$$

where $0 \leq \lambda \leq 1$.

The weight factor $\lambda = 0$ and 1 corresponds to the explicit and implicit schemes, respectively. When the right half space in Fig. 1 is a perfect electric conductor(PEC), we easily find that E_y^{n+1} and H_z^{n+1} will be approximated as

$$E_y^{n+1} \rightarrow -\frac{\lambda}{1 - \lambda} E_y^-, \qquad (2.6)$$

$$H_z^{n+1} \rightarrow \sqrt{\frac{\epsilon^+}{\mu^+}} \left[\left(1 + \frac{\sigma^+ \Delta t}{\epsilon^+} \right) E_y^+ + \sqrt{\frac{\mu^+}{\epsilon^+}} H_z^+ + \frac{\lambda}{1 - \lambda} E_y^- \{ 1 + \frac{\sigma^+ \Delta t}{\epsilon^+} (1 - \lambda) \} \right]. \quad (2.7)$$

In such a case, E_y^{n+1} and H_z^{n+1} are unstable with the explicit scheme($\lambda = 1$) for PEC. Therefore, we should employ the implicit scheme($\lambda = 0$) according to Beggs, and E_y^{n+1}

and H_z^{n+1} are obtained as

$$E_y^{n+1} = \frac{1}{\Omega} \left\{ \sqrt{\frac{\epsilon^+}{\mu^+}} E_y^+ + \sqrt{\frac{\epsilon^-}{\mu^-}} E_y^- + H_z^+ - H_z^- \right\} \tag{2.8}$$

$$H_z^{n+1} = \frac{1}{\Omega} \left\{ \left(1 + \frac{\sigma^- \Delta t}{\epsilon^-}\right) \sqrt{\frac{\mu^+}{\epsilon^+}} H_z^+ + \left(1 + \frac{\sigma^+ \Delta t}{\epsilon^+}\right) \sqrt{\frac{\mu^-}{\epsilon^-}} H_z^- + \right.$$
$$\left. \left(1 + \frac{\sigma^- \Delta t}{\epsilon^-}\right) E_y^+ - \left(1 + \frac{\sigma^+ \Delta t}{\epsilon^+}\right) E_y^- \right\} \tag{2.9}$$

where

$$\Omega := \sqrt{\frac{\epsilon^+}{\mu^+}} \left(1 + \frac{\sigma^+ \Delta t}{\epsilon^+}\right) + \sqrt{\frac{\epsilon^-}{\mu^-}} \left(1 + \frac{\sigma^- \Delta t}{\epsilon^-}\right).$$

For the TM mode, E_z^{n+1} and H_y^{n+1} can be similarly described as follows.

$$E_z^{n+1} = \frac{1}{\Omega} \left\{ \sqrt{\frac{\epsilon^+}{\mu^+}} E_z^+ + \sqrt{\frac{\epsilon^-}{\mu^-}} E_z^- + H_y^- - H_y^+ \right\}, \tag{2.10}$$

$$H_y^{n+1} = \frac{1}{\Omega} \left\{ \left(1 + \frac{\sigma^- \Delta t}{\epsilon^-}\right) \sqrt{\frac{\mu^+}{\epsilon^+}} H_y^+ + \left(1 + \frac{\sigma^+ \Delta t}{\epsilon^+}\right) \sqrt{\frac{\mu^-}{\epsilon^-}} H_y^- \right.$$
$$\left. - \left(1 + \frac{\sigma^- \Delta t}{\epsilon^-}\right) E_z^+ + \left(1 + \frac{\sigma^+ \Delta t}{\epsilon^+}\right) E_z^- \right\}. \tag{2.11}$$

Since the upstream points $(E_y, B_z)^\pm$ or $(E_z, B_y)^\pm$ are not always located at the grid points, we need to employ some interpolations to predict the profile inside the grid cell. Beggs employed two kinds of quadratic-Lagrange interpolation with the second-order accuracy in time and space $O\left(\Delta t^2, \Delta x^2\right)$ (hereafter QUL1,2 in Ref. [10]). The upstream value can be obtained as $f (= E_y, H_z)^\pm = f_{QUL1,2}^\pm (x_i - c^\pm \Delta t)$, where $f_{QUL1,2}^\pm (x)$ are the quadratic interpolations. It can be easily found by the Taylor expansion that the QUL has the equivalent order of accuracy as the FDTD method. On the contrary, since the CIP method uses the spatial derivative for interpolation, its time evolution is also required, which can be determined from the equations for spatial derivatives by taking a spatial derivative of Eqs. (2.8-2.9) or (2.10-2.11). Therefore, the upstream point can be obtained by the CIP as

$$f (= E_y, H_z)^\pm = f_{CIP}^\pm \left(x_i - c^\pm \Delta t\right) \tag{2.12}$$
$$\frac{\partial}{\partial x} f (= E_y, H_z)^\pm = \frac{\partial}{\partial x} f_{CIP}^\pm \left(x_i - c^\pm \Delta t\right) \tag{2.13}$$

where $f_{CIP}^\pm (x)$ will be explicityly given later in Eq. (A.4). On the contrary, the cubic-Lagrange method(hereafter CUL) that uses four grid points is also able to keep the third order accuracy as the CIP. It is likely to imagine that there are few differences between

them, but the CIP has some advantages than the CUL as mentioned in our previous paper [7].

When the CIP-MOC is extended to multi-dimensions, Eqs. (2.8) to (2.11) are used by directional splitting in the x-direction because multi-dimensional Maxwell equations can be described by the combination of TE and TM modes. It will be discussed in section 3.

2.2 Numerical experiments in one dimension

2.2.1 Error analysis

One of the most important issues in the solution of the Maxwell equation is how error depends on the grid size. In this section, we shall compare the errors of the CIP-MOC, the FDTD method, the QUL1,2 and the CUL. Both the permittivity ϵ and permeability μ are constant($= 1.0$) and conductivity $\sigma = 0$ in homogeneous media. Therefore, the speed of light c is 1.0.

The smooth initial profile is used for error analysis in the TE mode:

$$E_y\left(x, t=0\right) = 1.0 + 0.5\exp\left\{-\left(\frac{x-x_c}{h}\right)\right\},$$
$$E_y = H_y = H_z\left(x, t=0\right) = 0.0, \tag{2.14}$$

where $x_c = X_{max}/2 = 1.0$ and $h = 0.1$. The grid size is $\Delta x = X_{max}/NX$, where NX is the number of grid, and CFL $\equiv c\Delta t/\Delta x$ is fixed to 0.2. The error is defined as

$$err \equiv \sum_{i=1}^{NX}\left|\frac{E_{y(CIP)} - E_{y(Exact)}}{E_{y(Exact)}}\right|/NX. \tag{2.15}$$

We examine the accuracy of each method by calculating error (2.15) changing the number of grid NX, in other words, changing the grid size $\Delta x = X_{max}/NX$.

Fig. 2 shows the propagation of electric field solved by the CIP-MOC and the FDTD method with $NX = 400$. We can hardly see the differences between the CIP-MOC and the FDTD because the initial profile is very smooth. This means that when we deal with smooth profile, in other words, if we use sufficiently fine mesh, both the CIP-MOC and the FDTD can reproduce the correct result. Needless to say, the same can be said of the other schemes, QUL1,2 and CUL.

In view of Fig. 3, however, the error analysis of the result at $t = 0.4$ shows that the CIP and the CUL are the third-order while FDTD and QUL1,2 are the second-order in time and space. What is interesting in Fig. 3 is that the accuracy of the QUL is lower than the FDTD, while both schemes are second-order accurate in time and space.

Although both the CIP and the CUL are the third-order schemes in time and space, the error of the CIP is almost one-order of magnitude better than of the CUL. This result agrees with our previous paper that deals with the shallow water equations [7]. This suggests that the discussion on the accuracy should be made in terms of absolute value of
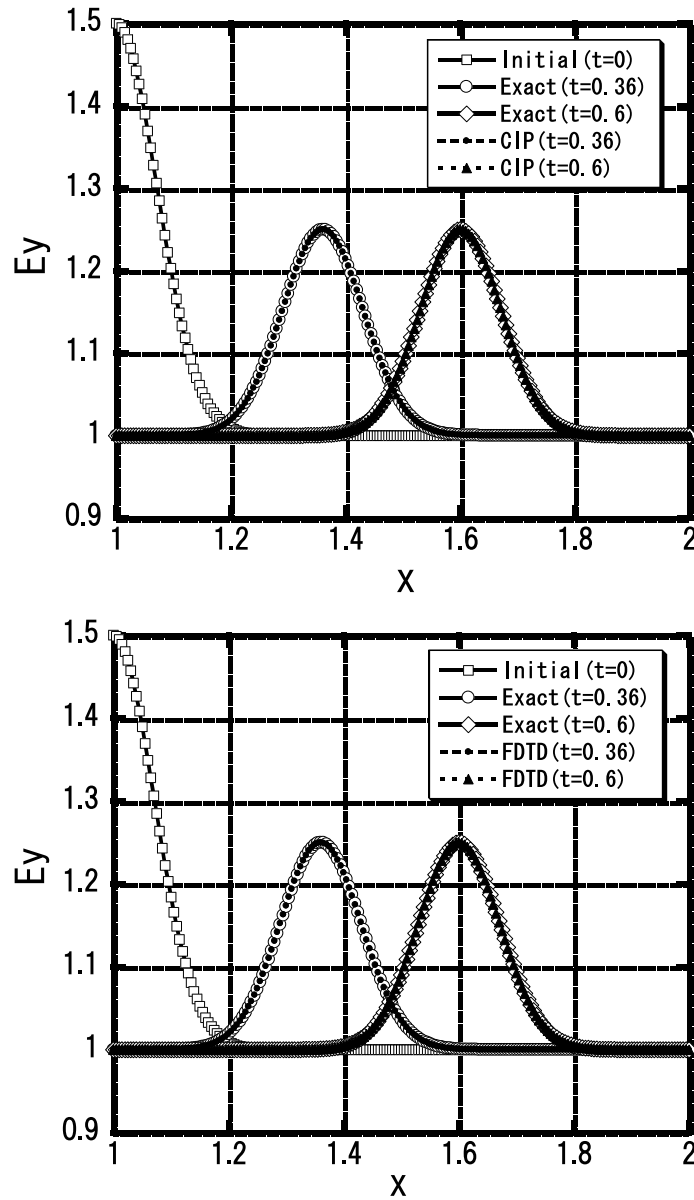
Figure 2: The propagation of E_y. Top: CIP, Bottom: FDTD. The number of mesh is $NX = 400$.

errors as well as the dependency on the grid size. Suppose the error of 10^{-4} for example, the CIP is capable of simulating with almost one-order of magnitude coarser mesh size than the QUL. This difference is significant because it becomes three-orders of magnitude in three dimensions. Thus we expect significant reduction of grid numbers compared with the QUL and the FDTD.
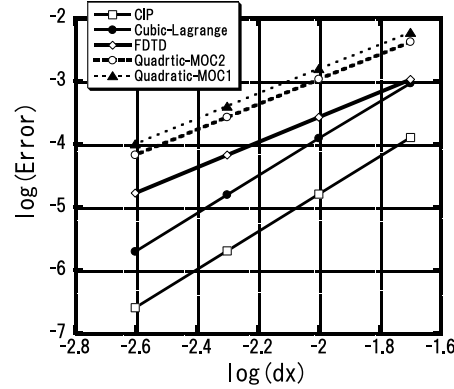
Figure 3: The error analysis. The error is defined by Eq. (2.15).

2.2.2 Phase error

When we consider a smooth profile, the CIP-MOC method is proven to have the smallest error. In order to show the further superiority of the CIP-MOC method to the other schemes in views of phase error, the advection of a rectangular wave is examined.

The phase error of MOC on the basis of Lagrange interpolation was discussed in previous papers [6, 13], and it can be readily predicted that the CIP is better than the CUL and the QUL1,2. In this section, we add the comparison with the FDTD method.

The initial electric field is a rectangular wave, and the magnetic field is zero:

$$E_y\left(x, t = 0\right) = \left\{ \begin{array}{ll} 1.0 & 0.4 < x < 0.6 \\ 0.0 & \text{otherwise} \end{array} \right. , \quad H_z\left(x, t = 0\right) = 0.0 \tag{2.16}$$

The number of meshes is $NX = 200$, and CFL$(= c\Delta t / \Delta x)$ is fixed to 0.2. Fig. 4 shows the results of the CIP and the FDTD at $t = 0.25$. While the FDTD has a large numerical oscillation around discontinuities, the CIP is able to completely maintain the rectangular shape. This comes from phase error of the FDTD, in other words, the phase speed of FDTD has a sensitive dependence on the wavelength. It can be seen in Fig.5 that depicts the phase error of the CIP and the FDTD. The phase speed of the FDTD is not zero even for $k\Delta x = \pi$ (cutoff frequency), but it is about 40% smaller than the exact phase speed for $k\Delta x = \pi$. On the other hand, the CIP can solve such rectangular wave as well as smooth profile since the phase error of the CIP is very small for all wavenumbers.

Although this test may not make sense because wave profiles are in general smooth , it is worth while considering this example carefully. The rectangular wave includes all the wavelength, which can be easily understood by the Fourier transform. Therefor the above example proves that the CIP-MOC is able to treat all the wavelength components with small number of meshes. Such advantage of the CIP should become more important in multi-dimensions because the domain scale is usually much larger than the wavelength and we need to make the grid size for one wave length as large as possible. Generally speaking,
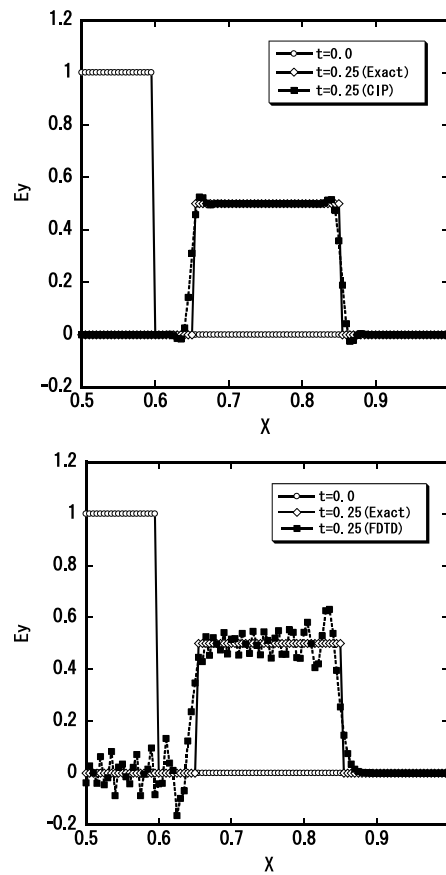
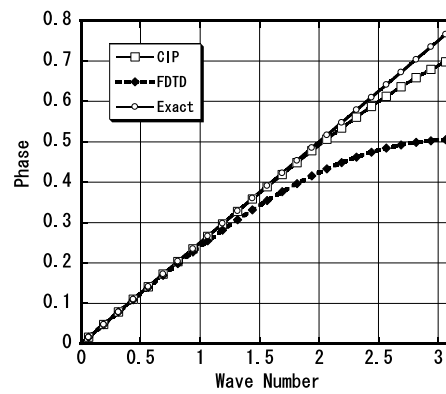Figure 4: Propagation of rectangular wave E_y at $t = 0.25$. Top: CIP, Bottom: FDTD.

Figure 5: Phase error of the CIP and the FDTD.

electromagnetic waves consist of all kinds of frequency. If we try to reduce the number of grid in the FDTD, such dispersion will cause the different wave speed depending on the wavelength. Therefore, the CIP-MOC has a large potentiality for all kinds of practical applications.

3   Maxwell equations in multi-dimensions

3.1   Introduction

In Section 2, the fundamental concept of CIP-MOC for the Maxwell equations in one-dimensional case was outlined. Next issue is to extend the CIP-MOC to the multi-dimensional scheme.

The Maxwell equations in three dimensions can be similarly written in a vector-martix form

$$\frac{\partial \mathbf{W}}{\partial t} + A(\mathbf{W})\frac{\partial \mathbf{W}}{\partial x} + B(\mathbf{W})\frac{\partial \mathbf{W}}{\partial y} + C(\mathbf{W})\frac{\partial \mathbf{W}}{\partial z} + \mathbf{F} = 0, \tag{3.1}$$

where $\mathbf{W} = (E_x, E_y, E_z, H_x, H_y, H_z)$ is the electromagnetic field vector components. $\mathbf{F}$ includes other effects like electrical resistance, current source $\mathbf{J}$, and so on. If the current follows Ohm's law, we can set $\mathbf{J} = \sigma\mathbf{E}$ where σ is the electrical conductivity.

If the Maxwell equations(3.1) can be represented by the combinations of three-dimensional advection equations, in other words, some characteristics like

$$\sum_l \alpha^l \frac{D^l f^l}{Dt} = A, \quad \frac{D^l f^l}{Dt} \equiv \frac{\partial}{\partial t} + u^l \frac{\partial}{\partial x} + v^l \frac{\partial}{\partial y} + w^l \frac{\partial}{\partial z} \tag{3.2}$$

the multi-dimensional CIP can be applied to the left hand side, where f^l is each component of electromagnetic field. Unfortunately, however, we are not able to find an expression with $A = 0$ in multi-dimensional Maxwell equations but only get the form with $A \neq 0$, which means a non-advection term is unavoidable on the right hand side. This is called the bi-characteristics method, which has been usually used for hydrodynamics in two dimensions. When we extend the bi-characteristics method to three dimensions for the Maxwell equations, however, the equations for variables should be very complicated and the equations for the spatial gradients used for the CIP must be much more complicated than for the variables. In addition, the accuracy or the symmetry would be severely deteriorated unless the right hand side $A \neq 0$ could be accurately estimated . Therefore, the bi-characteristics method does not seem to be practical. In order to resolve such difficulty, the CIP-MOC is applied to Eq. (3.1) with directional splitting . Since we have already established the CIP-MOC with directional splitting for the shallow water equations in two dimensions [7] and the Maxwell equations (3.1) have the same form as the shallow water equations, we will be able to establish the Maxwell solver by a similar procedure.

3.2 Method of characteristics with directional splitting

We can establish the general multi-dimensional CIP-MOC in heterogeneous dielectrics and conductors for the Maxwell equations, that is, $\mathbf{F} \neq 0$ in heterogeneous media in Eq. (3.1). In order to use the directional splitting method, Eq. (3.1) is split into a pair of one-dimensional operators:

$$\frac{\partial \mathbf{W}}{\partial t} + A(\mathbf{W})\frac{\partial \mathbf{W}}{\partial x} = \frac{1}{3}\mathbf{F} \quad \mathbf{W}^n \to \mathbf{W}^* : L_x \tag{3.3}$$

$$\frac{\partial \mathbf{W}}{\partial t} + B(\mathbf{W})\frac{\partial \mathbf{W}}{\partial y} = \frac{1}{3}\mathbf{F} \quad \mathbf{W}^* \to \mathbf{W}^{**} : L_y \tag{3.4}$$

$$\frac{\partial \mathbf{W}}{\partial t} + C(\mathbf{W})\frac{\partial \mathbf{W}}{\partial z} = \frac{1}{3}\mathbf{F} \quad \mathbf{W}^{**} \to \mathbf{W}^{n+1} : L_z \tag{3.5}$$

Hereafter, the operators of each direction is represented by L_x, L_y and L_z, respectively. It should be noted that the factor $1/3$ is required in the calculation of $\mathbf{F}$ on the right hand side because the effect of $\mathbf{F}$ is distributed to each-direction equally in three dimensions.

Each direction can be solved by the same procedure as one dimension. For example, Eq. (3.3) in the x-direction has six equations like

$$\frac{\partial E_y}{\partial t} + \frac{1}{\epsilon}\frac{\partial H_z}{\partial x} = -\frac{1}{3}\frac{\sigma}{\epsilon}E_y, \quad \frac{\partial H_z}{\partial t} + \frac{1}{\mu}\frac{\partial E_y}{\partial x} = 0, \tag{3.6}$$

$$\frac{\partial E_z}{\partial t} - \frac{1}{\epsilon}\frac{\partial H_y}{\partial x} = -\frac{1}{3}\frac{\sigma}{\epsilon}E_z, \quad \frac{\partial H_y}{\partial t} - \frac{1}{\mu}\frac{\partial E_z}{\partial x} = 0, \tag{3.7}$$

$$\frac{\partial E_x}{\partial t} = -\frac{1}{3}\frac{\sigma}{\epsilon}E_x, \qquad \frac{\partial H_x}{\partial t} = 0. \tag{3.8}$$

The pairs (E_y, H_z) in Eq. (3.6) and (E_z, H_y) in Eq. (3.7) are combined to make the two one-dimensional characteristics as in Eq. (2.3), then Eqs. (3.6) and (3.7) is reduced to

$$\frac{D^{\pm}E_y}{Dt} \pm \sqrt{\frac{\mu}{\epsilon}}\frac{D^{\pm}H_z}{Dt} = -\frac{1}{3}\frac{\sigma}{\epsilon}E_y, \tag{3.9}$$

$$\frac{D^{\pm}E_z}{Dt} \mp \sqrt{\frac{\mu}{\epsilon}}\frac{D^{\pm}H_y}{Dt} = -\frac{1}{3}\frac{\sigma}{\epsilon}E_z, \tag{3.10}$$

where $C_x^{\pm} : D^{\pm}/Dt = \partial/\partial t + c^{\pm}\partial/\partial x$. These equations (3.9) and (3.10) are almost the same as Eq. (2.3) except for the factor $1/3$. Therefore, $(E_y, H_z)^*$ and $(E_z, H_y)^*$ can be obtained by Eqs. (2.8), (2.9) and Eqs. (2.10),(2.11), respectively in the x-direction, where * means the temporal values. As for $(E_x, H_x)^*$ in Eq. (3.8), H_x is constant and E_x can be updated by the implicit scheme for the operator L_x

$$E_x^* = \frac{E_x^n}{1 + \frac{\Delta t}{3}\frac{\sigma_{i,j,k}}{\epsilon_{i,j,k}}}, \quad H_x^* = H_x^n \tag{3.11}$$

where $\sigma_{i,j,k}$ and $\epsilon_{i,j,k}$ are the conductivity and permittivity at the grid (i,j,k). Eq. (3.11) is also able to treat PEC approximation ($E_x \to 0$ as $\sigma_{i,j,k} \to \infty$).

   Although the derivative $\partial_x f$ is solved by the CIP in the x-direction, the time evolution of transverse derivatives $\partial_y f$ and $\partial_z f$ cannot be obtained from one-dimensional CIP. Aoki proposed to use $\partial_x \partial_{y(,z)} f$ so that the CIP can also be applied to $\partial_{y(,z)} f$, which is called Type-C scheme [12]. However, we shall adopt linear interpolation instead of the CIP for only the translation of transverse derivatives $\partial_y f$ and $\partial_z f$ in the x-direction:

$$
f^*_{y(,z)i,j} = \begin{cases}
\partial_{y(,z)} f_{i,j} - \dfrac{\partial_{y(,z)} f_{i,j} - \partial_{y(,z)} f_{i-1,j}}{\Delta x} \lambda_x \Delta t, & \lambda_x > 0 \\[4mm]
\partial_{y(,z)} f_{i,j} + \dfrac{\partial_{y(,z)} f_{i,j} - \partial_{y(,z)} f_{i+1,j}}{\Delta x} \lambda_x \Delta t, & \lambda_x < 0.
\end{cases}
\tag{3.12}
$$

where λ_x is the characteristic speed (equal to the speed of light $= \pm c$ in the Maxwell equations). This scheme is called Type-M scheme [11]. It was proved in Ref. [8] that the accuracy of Type-M is slightly lower than the Type-C that has the third-order accuracy. Since Type-M does not have to use additional variables like $\partial_{yz} f, \partial_{xyz} f$, it will help us reducing memories and calculation times, especially it is very effective for three-dimensional large-scale calculations. In addition, Type-M was also shown to give adequate results in the shallow water equations in our previous paper. Therefore we shall use Type-M scheme in this paper.

   As for the next step towards the y and z-direction, the same procedure as the x-direction is applied. For example, $(E_z, H_x)^{**}$, $(E_x, H_z)^{**}$ and their spatial derivatives are obtained by the CIP-MOC ($\partial_y f$ is solved by CIP and $\partial_{(x,z)} f$ are by Eq. (3.12)) and $(E_y, H_y)^{**}$ is obtained in a form similar to Eq. (3.11) in the y-direction. The extension to three dimensions is straightforward.

   Shang proposed an implicit and explicit fractional-step methods for solving 3D, timedependent Maxwell equations [14]. The coefficient matrices A, B and C in Eq. (3.1) have the eigenvalues, and they may be independently diagonalized by a straightforward matrix multiplication. The present scheme might be recognized to be some extension of some concepts of both Shang and Beggs schemes to general Maxwell solver with the CIP method.

   Important difference of the CIP-MOC is that the formulas for directional operators Eqs. (3.3) to (3.5) can be explicitly determined by using only some combinations of one-dimensional formula like Eq. (2.3), and it is very easy for the CIP-MOC to be extended to arbitrary grid system like the Soroban grid because the CIP is a compact scheme.

4 Plane-wave scattering by a perfectly conducting circular cylinder

As the multi-dimensional example, plane-wave scattering by a perfectly-conducting circular cylinder in an isotropic and homogeneous medium is examined. This is a classical problem and its solution can be found in several books of fundamental electromagnetism [15,16].
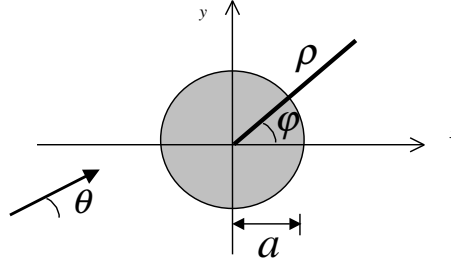
Figure 6: Geometry of the problem and notation. a is the cylinder radius and $\rho \equiv \sqrt{x^2 + y^2}$, $\varphi = \arctan(y/x)$.

When a plane wave is incident on a perfectly-conducting circular cylinder, the scattered wave is generated, then the total field can be expressed as the sum of two waves. The latter can be expanded in terms of cylindrical functions, which are defined as the product of a Hankel function of the second kind of integer order $H_n^{(2)}$ times a sinusoidal angular factor $\exp(jn\theta)$, where $j \equiv \sqrt{-1}$ and θ is the angle of wave vector. The time dependency is assumed to be $\exp(j\omega t)$, where ω is the angular frequency.

In the following sections, we compare the CIP-MOC and the FDTD method for a plane wave (TM mode or TE mode) coming from the left direction with angle $\theta = 0$, and the perfectly conducting circular cylinder (gray circle) shown in Fig. 6 is placed at the center.

4.1 TM mode

The initial TM plane wave having the components E_y and H_z is set for CIP-MOC and FDTD simulations as

$$E_z^{inc}(x, y, t = 0) = \cos\left(\frac{2\pi x}{\lambda}\right), \quad H_y^{inc}(x, y, t = 0) = -\sqrt{\frac{\epsilon_0}{\mu_0}} E_z^{inc}, \quad \text{if } 0 \le x \le 2\lambda;$$

$$E_z^{inc}(x, y, t = 0) = H_y^{inc}(x, y, t = 0) = 0, \qquad \text{otherwise} \qquad (4.1)$$

where both ϵ_0 and μ_0 are normalized to 1.0 in free space. Two kinds of the number of grid are employed, $(NX, NY) = (100, 60)$ as coarse grid and $(NX, NY) = (200, 120)$ as fine grid for comparison. The grid spacing is $\Delta x = \Delta y = 1.0/NX$. The time step $\Delta t = 0.1\Delta x$ corresponds to CFL=0.1. The radius of the PEC cylinder a is 0.1 and the wavelength λ is equal to the cylinder diameter ($= 2a = 0.2$), which corresponds to $ka = \pi$.

Fig. 7 shows the comparison of E_z contours among (a) the exact solution, (b) CIP and (c) FDTD at $t = 1.0$. The grid is uniform in both schemes and the number of grid is $(NX, NY) = (100, 60)$. Both CIP-MOC and FDTD agree well with the exact solution on the whole. However, the diffracted wave in $x > 0.5$ and reflected wave $x < 0.5$ of CIP seem closer to the exact solution than of FDTD but both results seem to be partly different from the exact solution.

In order to improve these results, the Soroban grid is used for the CIP-MOC. The Soroban grid consists of planes, lines and grid points. The grid points are constrained to move along the lines and lines are constrained to move on the planes [8]. The number of
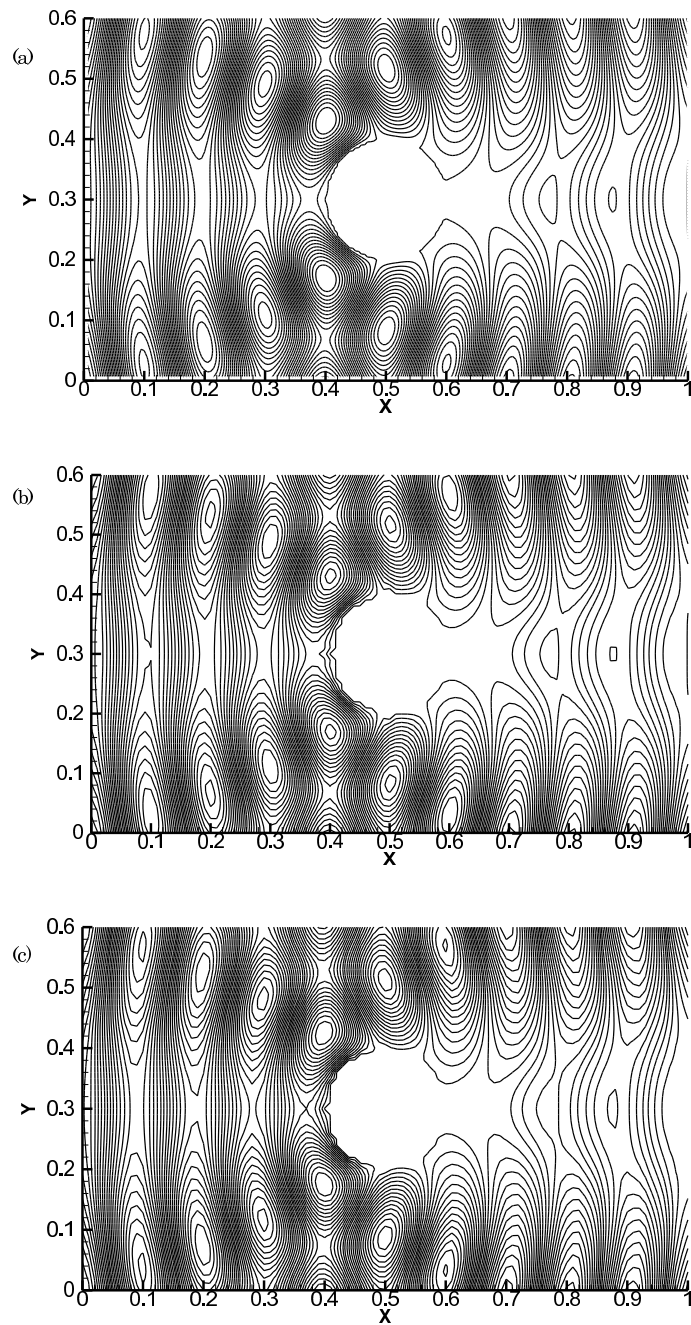
Figure 7: The comparison of E_z at $t = 1.0$. (a): Exact solution, (b): CIP, (c): FDTD in uniform mesh. -1.7 to 1.7, 25 split, 0.25 thick.
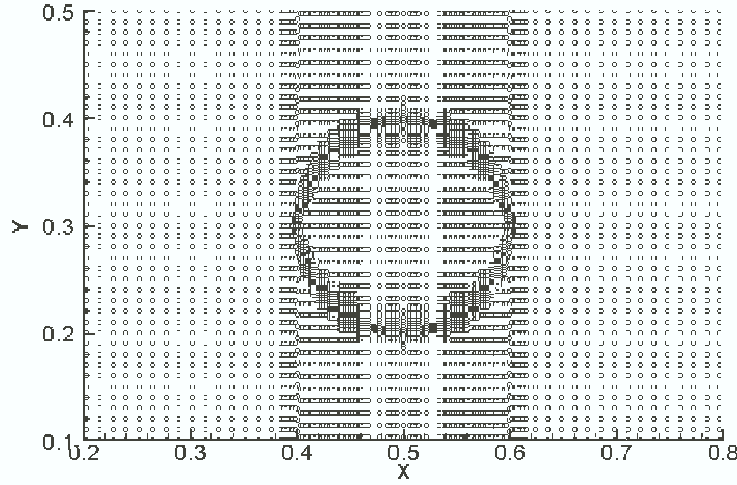
Figure 8: The Soroban grid around the cylinder. The number of lines is 100 and 60 points are on each line.

lines is 100 and 60 points are placed on each line. Therefore, the number of grid is also 6000 that is the same as uniform mesh in Fig.7 (Hereafter, NX means the number of lines and NY means the number of grid points on each line in the Soroban grid for the sake of convenience). The Soroban grid used in the CIP-MOC is displayed in Fig. 8.

The lines and grid points on the lines are concentrated around the cylinder surface in the Soroban grid. The grid spacing of the Soroban grid in the region far from the cylinder is coarser than uniform mesh because lines are concentrated at the cylinder surface, while the number of grid is the same as coarse uniform grid. In the calculation, the ratio of the maximum to minimum grid spacings was five. It must be very hard to calculate complex surface boundary with the Cartesian grid like that used in the FDTD, even if sub-grid method or sub-cell method could be used. For comparison, the fine uniform mesh $(NX, NY) = (200, 120)$ is employed for the FDTD.

Fig. 9 shows the E_z contours of the CIP-MOC with the Soroban grid, the FDTD with fine grid and the exact solution. The results of the CIP-Soroban and the FDTD become better than Fig. 7 and they are almost identical to the exact solution. Especially, the Soroban grid makes the scattered wave near the cylinder shaper than uniform mesh even though the number of grid points is the same as Fig. 7. In the contours, it might be very hard to recognize the difference of these schemes.

Fig. 10 shows the cross section of reflected wave $(0.05 \le x \le 0.45)$, diffracted wave $(0.55 \le x \le 1.0)$ in the x-direction, and the y-direction $(0 \le y \le 0.3)$ because the result is symmetrical at $y = 0.3$.

The results of the CIP-MOC and the FDTD are almost identical to the exact solution except for Fig. 10(a) because the profile is relatively smooth on the right side of the cylinder $(x > 0.6)$ and hence the FDTD is also able to solve the diffracted wave. The CIP with uniform mesh $(NX, NY) = (100, 60)$ is almost the same as the FDTD with
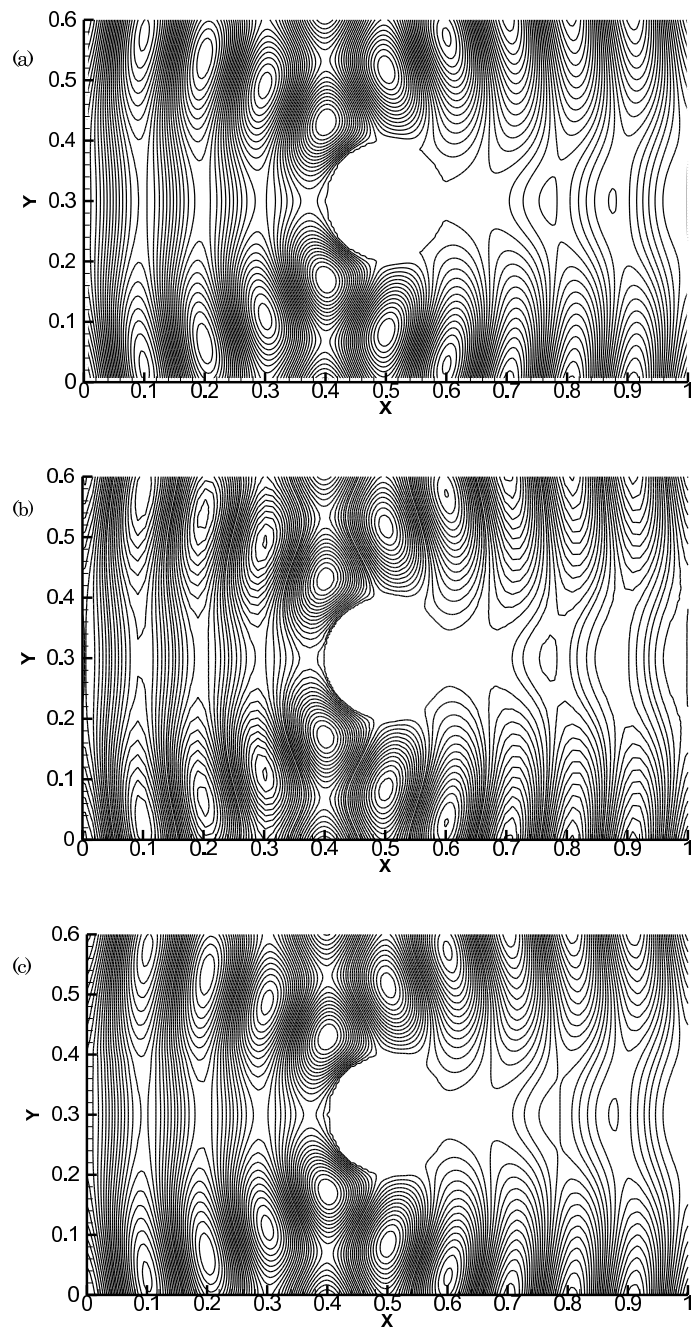
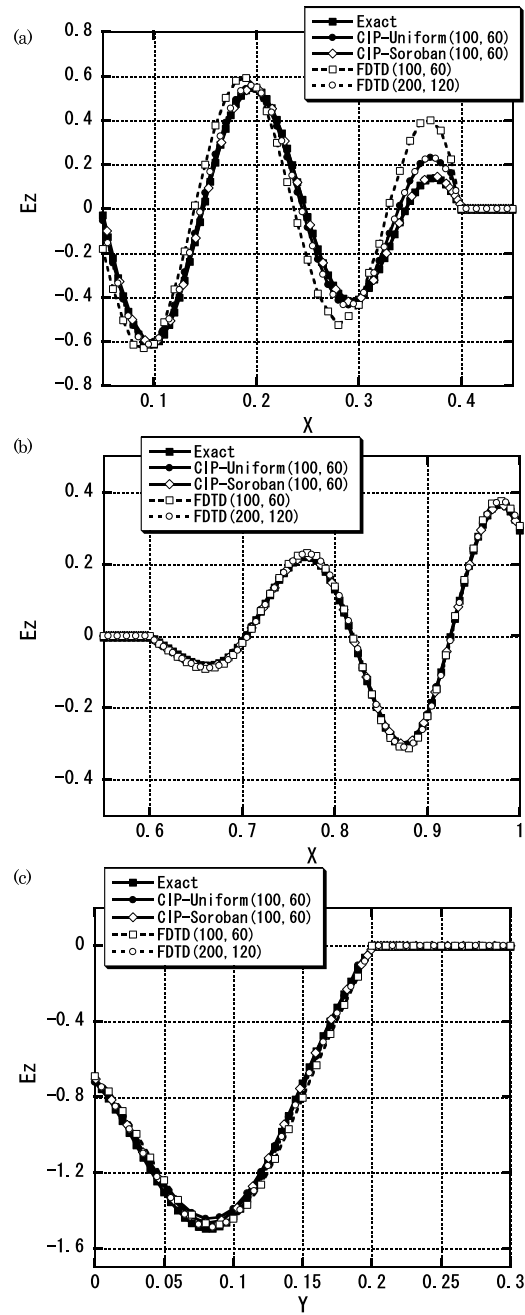Figure 9: The comparison of E_z at $t = 1.0$. (a): Exact solution, (b): CIP-Soroban, (c): FDTD-fine.

Figure 10: The cross section of E_z in the x-direction at $y = 0.3$. (a): $(0 \le x \le 0.45)$, (b): $(0.55 \le x \le 1.0)$ and (c): in the y-direction $(0 \le y \le 0.3)$.

$(NX, NY) = (200, 120)$. As shown in Fig. 10(a), however, the reflected wave of FDTD with $(NX, NY) = (100, 60)$ is two times larger than the others, and the reflected wave is a little bit out of phase .

There may be two reasons for such results. First one is due to the treatment of boundary condition at the cylinder in the FDTD and it implies that the simple Yee scheme is inadequate for the PEC if the grid resolution is not sufficient. Secondly, spatial derivative of E_y at the cylinder surface is not continuous while the value is continuous. Since this discontinuity can cause the phase error of the FDTD at the surface, the amplitude of reflected wave becomes larger. This result means that if the resolution around the cylinder (or the arbitrary body) is not enough, reflected wave can be incorrect that should affect the whole distribution. It should be noticed that the FDTD gives two times larger reflection wave even for the case in which one wavelength is described by 15-20 grid points. The CIP-MOC with the Soroban grid is able to give the result better than the FDTD with fine grid and completely identical to the exact solution even though the number of grid is the same as uniform mesh $(NX, NY) = (100, 60)$.

4.2   TE mode

The second case is the TE mode. The initial TE plane wave having the components E_y and H_z is set as

$$E_y^{inc}(x, y, t = 0) = \cos\left(\tfrac{2\pi x}{\lambda}\right), \ H_z^{inc}(x, y, t = 0) = -\sqrt{\tfrac{\epsilon_0}{\mu_0}} E_y^{inc} \quad \text{if } 0 \le x \le 2\lambda;$$

$$E_y^{inc}(x, y, t = 0) = H_z^{inc}(x, y, t = 0) = 0 \qquad\qquad \text{otherwise} \qquad (4.2)$$

The number of grid is the same as the TM mode, that is, the CIP-MOC with uniform grid and Soroban grid is $(NX, NY) = (100, 60)$, and the FDTD employs two sets of grid points $(NX, NY) = (100, 60)$ and $(NX, NY) = (200, 120)$.

Fig. 11 shows the cross section of H_z profile. As in the TM mode, the CIP is closer to the exact solution for coarse mesh and becomes much closer when the Soroban grid is used.

It is shown in the previous section that both the CIP-MOC and the FDTD are able to obtain relatively accurate result for electric field on the whole in the TM mode. This is because the electric field is always zero and continuous in terms of values on the PEC boundary. However, since large discontinuous of the magnetic field can be generated on the PEC boundary, it becomes more difficult to deal with the magnetic field than the electric field.

It is very important to treat the vicinity of material surface with high resolution because the coarse mesh will generate incorrect scattered waves and the whole solution will be affected. Since the whole solution can be described by the sum of incident wave and scattered wave , the Soroban grid that can concentrate the grid points near the surface is very useful for the Maxwell equations.

The magnetic field of the CIP-MOC exists inside the PEC cylinder over a few meshes while there is no wave in the FDTD method. This is not because of the CIP but because
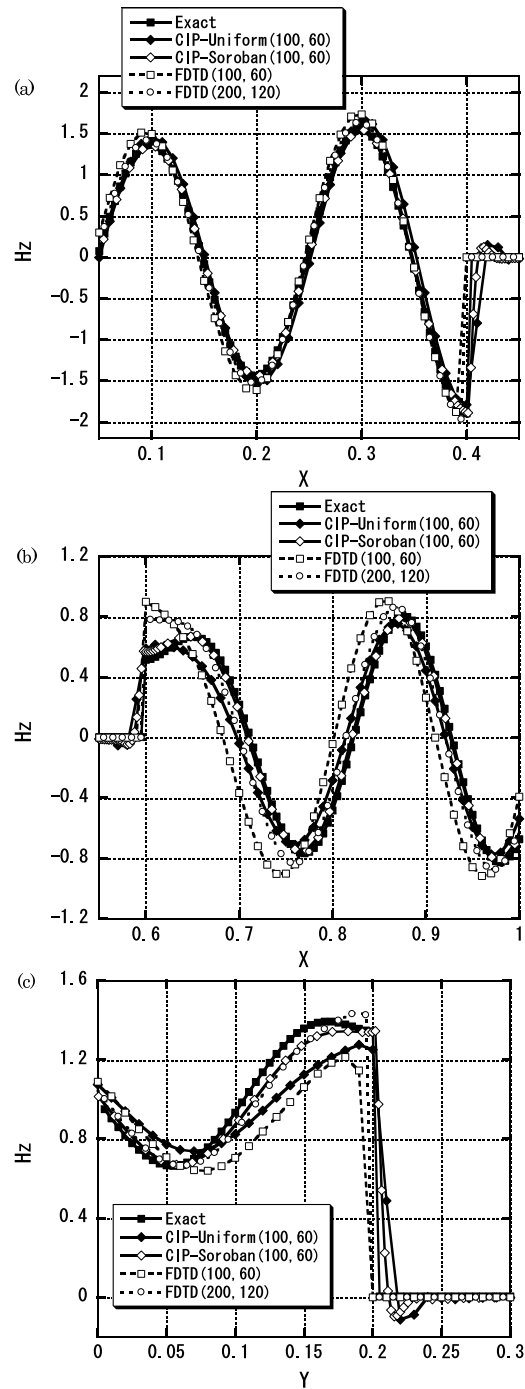
Figure 11: The cross section of H_z in the x-direction at $y = 0.3$. (a): $(0 \leq x \leq 0.45)$, (b): $(0.55 \leq x \leq 1.0)$ and (c): in the y-direction $(0 \leq y \leq 0.3)$.

of employing the MOC. Suppose the grid of PEC boundary is i in Fig. 1, as mentioned in Eqs. (2.6) and (2.7), $H_{z(i)}$ on the surface is not zero. Therefore, when $H_{z(i+1)}$ is calculated, it becomes non-zero since H_z^+ is obtained by an interpolation like the CIP, CUL and so on between $(i, i+1)$. Even though this effect will be rapidly reduced, the profile of magnetic field decays inside a PEC over a few meshes. On the contrary, the FDTD is based on the staggered mesh and hence $H_{z(i+1/2)}$ can always be zero, if the PEC boundary grid i is placed at the location of the electric field but not of the magnetic field.

Beggs suggested the PEC boundary condition for MOC, however, it should be noted that what we are really interested in is the solution outside of the PEC and the solution inside the PEC does not affect the outer solution. Such a behavior is observed only for the PEC but the calculation inside the cylinder becomes correct when the conductivity becomes smaller and the decay distance or skin depth in the conductor becomes the order of the grid size. Therefore, we can use Eqs. (2.9) for any conductivity but the special PEC boudary treatment is not necessary.

5   Application of Soroban grid to Vlasov equation

The Vlasov equation is used to describe the kinetic motion of charged particles in collision-less plasmas coupled with the Maxwell equation. The velocity distribution $f(\mathbf{x}, \mathbf{u}, t)$ is described by

$$\frac{\partial f}{\partial t} + \mathbf{u}\frac{\partial f}{\partial \mathbf{x}} + \frac{\mathbf{F}}{m}\frac{\partial f}{\partial \mathbf{u}} = 0. \tag{5.1}$$

where $\mathbf{F}$ is the force and m the mass. In three dimensions, this is the huge system and the distribution is described in six dimensional space. Since the CIP can describe the advection process accurately even with coarse grid, it enables us to directly solve six-dimensional phase space in Eulerian grid system. Actually, the Landau damping has been accurately calculated even with 10 grids in whole velocity space [18]. Furthermore, the exact particle conservation is guaranteed.

In most of the plasma simulations, the particle code is still the major group. This is because the particle velocities changed largely during the interaction with electromagnetic waves and thus the fixed Cartesian coordinate can not trace the dynamical acceleration. Since the accelerated velocities are different from space to space, we need a special mesh system in which velocity mesh varies in space. For that purpose, the Soroban grid is the most promising one.

In the following example, the lines are placed perpendicularly to the x-axis and the grid points move in the direction of velocity space. For testing the Soroban grid, we here used the free-streaming test in which $\mathbf{F} = 0$. The initial condition is

$$f(x, v, 0) = f_o(v)(1 + A\cos kx), \quad f_0(v) = \frac{1}{\sqrt{2\pi}}e^{-v^2/2}, \tag{5.2}$$

where we set $k = 0.5, A = 0.1$ and the system size in the x-direction is $L = 4\pi$ and the velocity space is from $v = -5$ to $v = 5$. The number of lines in the x-direction is 100 and
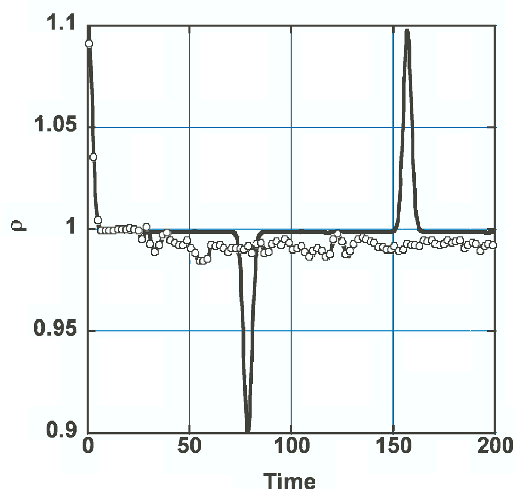
Figure 12: Time evolution of density. The solid line shows the fixed uniform grid and the circles for the Soroban grid.

the 64 grid points move along each line. The time step is fixed to 0.002.

It is well known that the recurrence phenomena occur when the finite difference method is used in the velocity space. Suppose the velocity space is uniformly divided. If the particle (=grid) with the lowest velocity reaches the periodic boundary $L = 4\pi$, the the particle with the second lowest velocity which is twice the lowest one traverses the system twice and also reaches the boundary. Thus all the particles reach sumultaneously at the boudary. This time is called recurrence time and all the phenomena should come back to the initial value.

Fig. 12 show the result of fixed uniform grid and the recurrence occurs at $t = 77.9$ as expected from the theory. Such recurrence is the key issues in employing the grid-based Vlasov solver. By using the Soroban grid shown in Fig. 13, the velocity grid is no more regular and we observed the dissapperance of the recurrence as shown in Fig. 12.

6   Conclusion

The new scheme for the Maxwell equations using the CIP-MOC in combination with Soroban grid is established in this paper. Since the CIP is less diffusive and has smaller phase error for advection equation, MOC is suitable for the CIP method. The CIP-MOC can be straightforwardly extended to multi-dimensional heterogeneous medias that include dielectrics and conductors by directional splitting.

In addition to the accuracy and low phase error mentioned in this paper, the CIP-MOC has some additional advantages compared to the finite difference schemes like the FDTD. In an open space, the incident wave or reflected waves by some objects should go though the free boundary. Since the CIP-MOC uses the characteristics, such a free boundary is
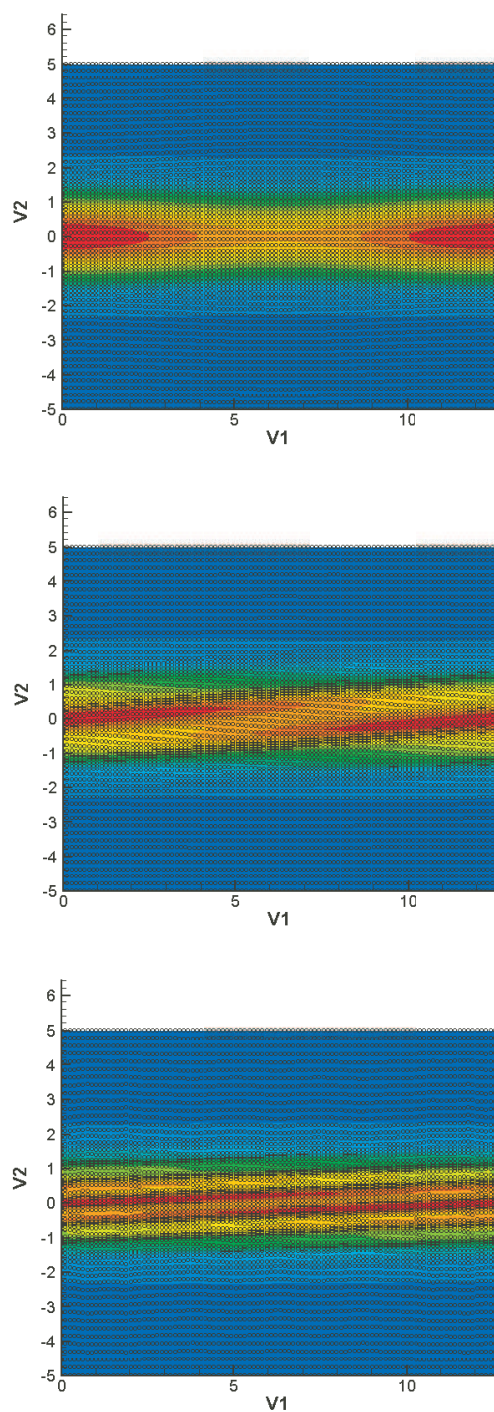
Figure 13: Soroban grid in phase space.

easily treated while some special treatments are required for the FDTD.

In the application of the Soroban grid, the key issue is how effectively locate the Soroban grid. Recently, Takizawa [17] has proposed an interesting ideas on how to make adequate Soroban grid near the surface of the body. The application of such idear will be published in future.

Appendix I : Principle of the CIP method

Let us review the numerical technique of the CIP method briefly. The one-dimensional form of the advection equation is given by

$$\frac{\partial f}{\partial t} + u\frac{\partial f}{\partial x} = 0. \tag{A.1}$$

When u is constant, if the initial condition of $f(x, t = 0) = F(x)$, the analytical solution of f can be easily described as $f(x, t) = F(x - ut)$, which means a simple translational motion of a wave. Even if u depends on x and t, this solution is approximately correct in a very short time Δt, that is, $f(x, t + \Delta t) \approx f(x - u\Delta t, t)$.

All kinds of semi-Lagrangian methods such as linear, quadratic Lagrange(QUL), cubic Lagrange(CUL), and so on employ a Lagrangian invariant solution. Therefore, the CIP method can be also called semi-Lagrangian scheme.

However, unlike conventional semi-Lagrangian schemes, the CIP method uses the spatial derivative of f as well, that is, Hermite spline interpolation. Let us differentiate Eq.(A.1) with spatial variable x, then we get

$$\frac{\partial g}{\partial t} + u\frac{\partial g}{\partial x} = -\frac{\partial u}{\partial x}g, \tag{A.2}$$

where g stands for the spatial derivative of f ($= \partial f/\partial x$). In the simplest case that the velocity u is constant, Eq.(A.2) coincides with Eq.(A.1) and represents the propagation of spatial derivative with a velocity u. By this equation, we can trace the time evolution of f and g on the basis of Eqs.(A.1) and (A.2).

If two values of f and g are given at two grid points, the profile between these points can be interpolated by cubic polynomial $F_{CIP}(x) = a_i x^3 + b_i x^2 + g_i x + f_i$. Thus, the profile at $n+1$ step can be obtained shifting the profile by $u\Delta t$ like $f^{n+1} = F(x - u\Delta t), g^{n+1} = dF(x - u\Delta t)/dx$. Suppose the case that the velocity u is negative, the coefficients (a_i, b_i) can be described as

$$a_i = \frac{g_i + g_{i+1}}{\Delta x^2} + \frac{2(f_i - f_{i+1})}{\Delta x^3}, \quad b_i = \frac{3(f_{i+1} - f_i)}{\Delta x^2} - \frac{2g_i + g_{i+1}}{\Delta x}, \tag{A.3}$$

and $(f_i, g_i)^{n+1}$ in the CIP can be obtained as

$$f_i^{n+1} = a_i X^3 + b_i X^2 + g_i^n X + f_i^n, \tag{A.4}$$

$$g_i^{n+1} = 3a_i X^2 + 2b_i X + g_i^n, \tag{A.5}$$

where we define $X = -u\Delta t$. On the other hand, f^{n+1} obtained by QUL1 and 2 is

$$f^{n+1}_{i(QUL)} = a_{i(QUL1,2)}X^2 + b_{i(QUL1,2)}X + f_i^n, \tag{A.6}$$

where the coefficients $\left(a_{i(QUL1,2)}, b_{i(QUL1,2)}\right)$ are

$$a_{i(QUL1)} = -\frac{(f_{i+1} - f_{i-1})\nu}{2}, \qquad b_{i(QUL1)} = \frac{(f_{i+1} - 2f_i + f_{i-1})\nu^2}{2} \tag{A.7}$$

$$a_{i(QUL2)} = -\frac{(3f_i - 4f_{i+1} + f_{i+2})\nu}{2}, \quad b_{i(QUL2)} = \frac{(f_i - 2f_{i+1} + f_{i+2})\nu^2}{2} \tag{A.8}$$

with ν the CFL number ($\equiv u\Delta t/\Delta x$). We can see that both QUL1 and QUL2 are the second-order schemes in time and space. The problem of the QUL2 is that it adds one downwind point, which provides a lagging phase error. This is in contrast to the upwind interpolation scheme in the CIP and the QUL1.

The CUL uses four values of grid points to make the cubic-polynomial as the CIP. Some fundamental comparisons between the CIP and CUL have already been performed in views of accuracy, phase error and so on, and some superiorities of the CIP were discussed in [7].

References

[1] K. S. Yee, Numerical solution of initial boundary value problems involving Maxwell's equations in isotropic media, IEEE Trans. Antennas Propagat., 14 (1966), 302-307.
[2] J. Jin, The Finite Element Method in Electromagnetics, IEEE Press, John Wiley & Sons Inc, 2002.
[3] H. Takewaki, A. Nishiguchi and T. Yabe, The cubic-interpolated pseudo-particle(CIP) method for solving hyperbolic-type equations, J. Comput. Phys., 61 (1985), 261-268.
[4] T. Yabe and T.Aoki, A universal solver for hyperbolic equations by cubic-polynomial interpolation, Comput. Phys. Commun., 66 (1991), 219-232.
[5] T. Yabe, T. Ishikawa, P. Y. Wang, T. Aoki, Y. Kadota and F. Ikeda, A universal solver for hyperbolic equations by cubic-polynomial interpolation II. Two- and three- dimensional solvers, Comput. Phys. Commun., 66 (1991), 232-242.
[6] T. Yabe, F. Xiao and T. Utsumi, The constrained interpolation profile method for multiphase analysis, J. Comput. Phys., 169 (2001), 556-593.
[7] Y. Ogata and T. Yabe, Multi-dimensional semi-Lagrangian characteristic approach to the shallow water equations by the CIP method, Int. J. Comput. Eng. Sci., 5(3) (2004), 699-730.
[8] T. Yabe, H. Mizoe, K. Takizawa, H. Moriki, H-N. Im and Y. Ogata, Higher-order schemes with CIP method and adaptive Soroban grid towards mesh-free scheme, J. Comput. Phys., 194 (2004), 57-77.
[9] G. R. Liu, Mesh Free Methods: Moving Beyond the Finite Element Method, CRC Press I Llc, 2002.
[10] J. H. Beggs, D. L. Marcum and S-L. Chan, The numerical method of characteristics for electromagnetics, Appl. Comput. Electromag. Soc. J., 14(2) (1999), 25-36.
[11] H. Takewaki and T. Yabe, Cubic-interpolated pseudo-particle(CIP) method applications to nonlinear or multi-dimensional problems, J. Comput. Phys., 70 (1987), 355-372.

[12] T. Aoki, Multi-dimensional advection of CIP (cubic-interpolated propagation) scheme, CFD J., 4 (1995), 279-291.

[13] T. Utsumi, T. Kunugi and T. Aoki, Stability and accuracy of the cubic interpolated propagation scheme, Comput. Phys. Commun., 101 (1996), 9-20.

[14] J. S. Shang, A fractional-step method for solving 3D, time-domain Maxwell equations, J. Comput. Phys., 118 (1995), 109-119.

[15] G. Cincotti, F. Gori and M. Santarsiero, Plane wave expansion of cylindrical functions, Opt. Commun., 95 (1993), 192-198.

[16] R. Borghi, F. Gori, M. Santarsiero, F. Frezza and G. Schettini, Plane-wave scattering by a perfectly conducting circular cylinder near a plane surface: Cylindrical-wave approach, J. Opt. Soc. Am. A., 13(3) (1996), 483-493.

[17] K. Takizawa, Numerical Scheme for Fluid Flow Including Moving Boundary and Complex Surface by Sorogan Grid CIP Method, Ph.D. Thesis, Tokyo Institute of Technology, Japan, 2005.

[18] T. Nakamura and T. Yabe, Cubic interpolated propagation scheme for solving the hyper-dimensional Vlasov-Poisson equation in phase space, Comput. Phys. Commun., 120 (1999), 122-154.